Coverage and binning issues for marine seismic surveys

Mundy Brink, Saga Petroleum, Sandvika, Norway
Shuki Ronen, Geco-Prakla, Gatwick, England

Downloaded 10/16/19 to 69.181.139.133. Redistribution subject to SEG license or copyright; see Terms of Use at http://library.seg.org/

To understand and quantify the impact of acquisition geometries on final processed data quality of marine 3-D seismic surveys, Saga Petroleum and Geco-Prakla initiated a study using a synthetic data set—three dipping layers (30°, 45°, and 60°) within a constant velocity medium below a water layer (Figure 1). A seismic experiment was simulated over this model along dip and strike directions. For each line, orientation swaths were acquired in two opposite directions: (1) for a simulated acquisition of adjacent sail lines in the same direction and (2) for adjacent sail lines in the opposite direction. The acquisition consists of 21 parallel streamers with a length of 4.5 km and a lateral streamer separation of 25 m. Additional data sets were generated by decimation of group interval and streamer separation and dual source geometry.

Experimental results. Cross-line stack sections and horizon slices were generated for different acquisition scenarios. Figures 2 and 3 show a cross-line of the 30°-dip event with conventional 3-D DMO with adjacent swaths in the same and opposite direction. In Figure 2 the central stack traces have significantly reduced amplitudes, since a portion of the subsurface is poorly illuminated. In contrast, Figure 3 shows that data generated with opposite swath directions produce a stack consisting of relatively uniform amplitudes.

Figure 4, inversion-to-zero offset (IZO, to be discussed below), seems, in comparison with Figure 2, to be superior in compensating for amplitude variations arising from 3-D DMO. Not shown here is the fact that AVO artifacts are generated due to the reduced far-offset coverage of updip reflectors. These are not resolved by IZO.

For data acquired with adjacent swaths in the same direction, conventional 3-D DMO can result in regions of poor subsurface illumination. It is recommended that sailing direction alternates between adjacent swaths. This is particularly important for AVO. For adjacent swaths in the same direction the application of IZO improves illumination in the shadow zones but does not solve the AVO artifacts.

Traditionally, the resolution of images obtained from seismic data is assumed limited by the nominal acquisition bin size. This is obvious, especially at the poststack stage, since the seismic images are sampled with the regular pattern of bin centers. At the prestack stage, the traces may have different offsets and azimuths. All of these are allocated to the nearest bin center in the regular bin pattern. This means that—due to the spatial filter implied by ignoring spatial distribution—potential resolution beyond the nominal bin size is lost.

Some of this spatial filter can be considered as a necessary antialias filter in connection with the spatial sampling. However, if the actual data distribution is honored correctly, improved spatial resolution can be achieved; i.e. a smaller bin size will yield improved resolution depending on the data distribution.

Relative to the present binning technique, prestack migration is claimed to better honor irregular acquisition geometries, yielding improved resolution. It often seems, however, that the increased spatial resolution is obtained at the expense of degraded wavelet fidelity and increased precursor noise. This is because prestack migration programs are based on the condition that the spatial sampling of the data allows wave equation integral operators to be implemented as summation of discrete sampling points. Violation of this condition results in artifacts and reduced fidelity. To provide this condition, a very strict specifica-

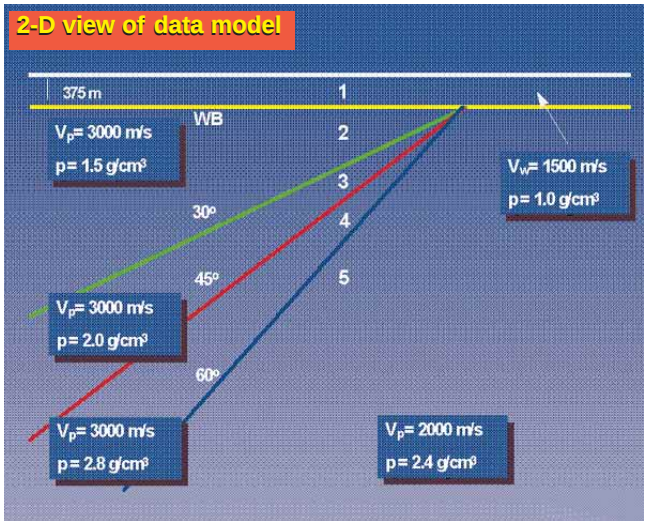

Figure 1. 2-D view of 3-D seismic model, containing water layer and three dipping interfaces (30°, 45°, and 60°).

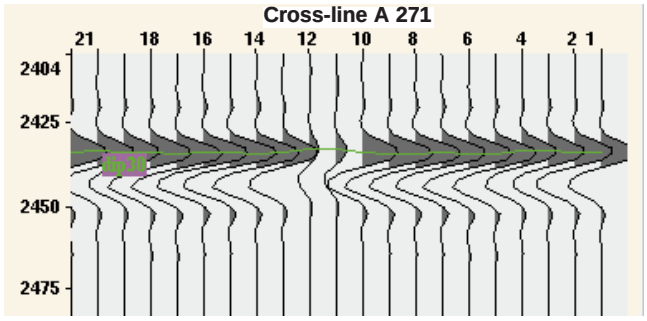

Figure 2. Cross-line of 30° dipping layer with 3-D DMO with swaths in the same direction.

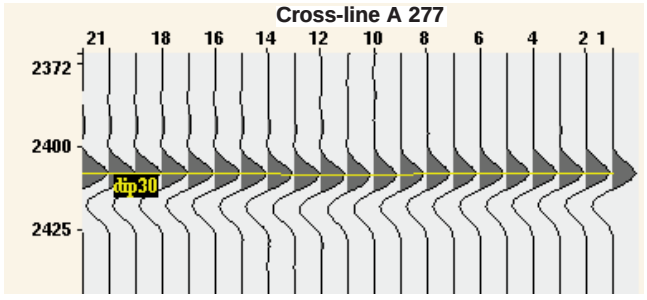

Figure 3. Cross-line of 30° dipping layer with 3-D DMO with swaths in the opposite direction

tion must be set to the actual acquisition geometry and data distribution.

IZO. Another technique, more robust than prestack migration for irregular acquisition geometry, is the previously mentioned IZO (Figure 5). Unlike migration, which is a forward processing technique, IZO is an inversion. No wavefield extrapolation operators are applied to irregularly sampled data. Prestack migration involves such extrapolation for downward continuation in depth. Partial prestack migration (also known as DMO) is based on an application of such operators inward in offset.

IZO is based on outward-offset continuation applied to an adequately sampled model. By iterative application of a well behaved extrapolation operator, IZO finds the optimum model that fits the irregularly distributed real data in the sense that the wave-equation operator applied to the model can reproduce the data.

With accurate positioning and IZO processing, one can turn binning error into a blessing. Instead of making an effort to concentrate all midpoints on bin centers, we will prefer to scatter the midpoints. As a consequence, we do not consider nominal bin size and fold coverage but look at spatial data density. Thus, instead of limiting the spatial resolution by the nominal bin size, we will obtain images with the full resolution achievable by the full frequency

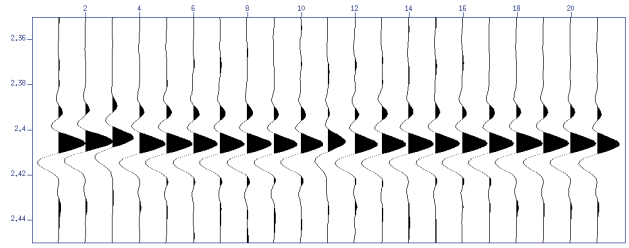

Figure 4. Cross-line of 30° dipping layer with IZO with swaths in the same direction.

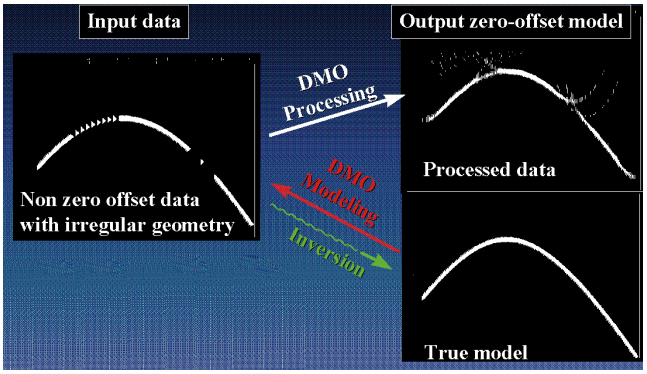

Figure 5. IZO technique. DMO processing of irregular data causes precursor artifacts. IZO is an iterative inversion technique and finds the optimum model in the sense that the wave equation operator applied to the regular model can reproduce the irregular data.

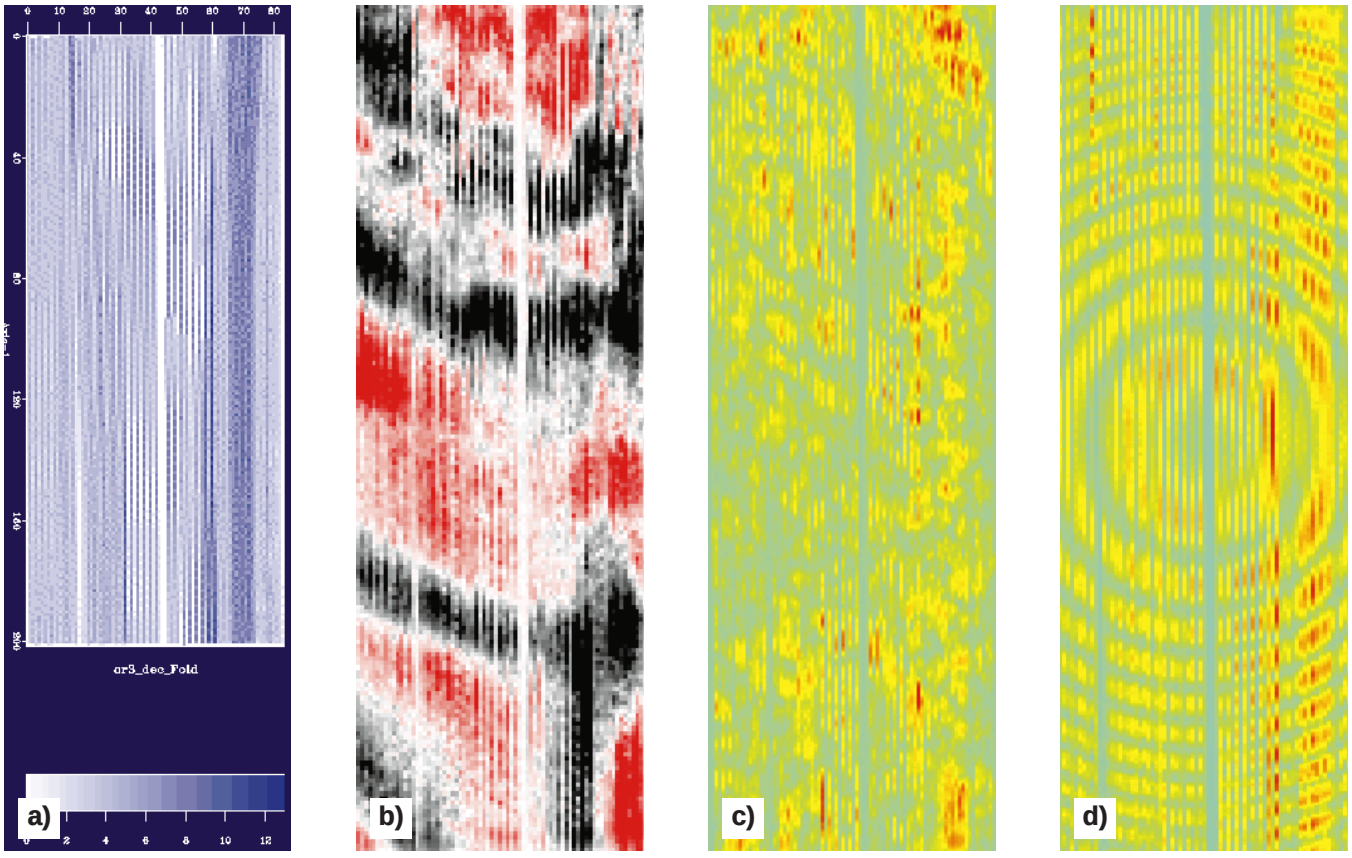

Figure 6. Bull's-eye coverage analysis. Geometry footprint in various domains. (a) Fold coverage map. The data include one offset band of 1000-1500 m. The nominal cross-line sampling is 25 m, but the required output grid is 12.5 m cross-line. (b) Time slice from DMO stack. (c) Frequency slice from the DMO-stack image of the real data. (d) Frequency slice from the DMO stack image of the synthetic data. The synthetic data were generated using the actual geometry of the real data. The earth model included a point diffractor and a flat reflector. The circles on the synthetic data image are due to the interference between the point diffractor and the flat reflector. The same geometry footprint can be seen in all four domains. The gap in the middle is about 50 m wide.

Downloaded 10/16/19 to 69.181.139.133. Redistribution subject to SEG license or copyright; see Terms of Use at http://library.seg.org/

Downloaded 10/16/19 to 69.181.139.133. Redistribution subject to SEG license or copyright; see Terms of Use at http://library.seg.org/

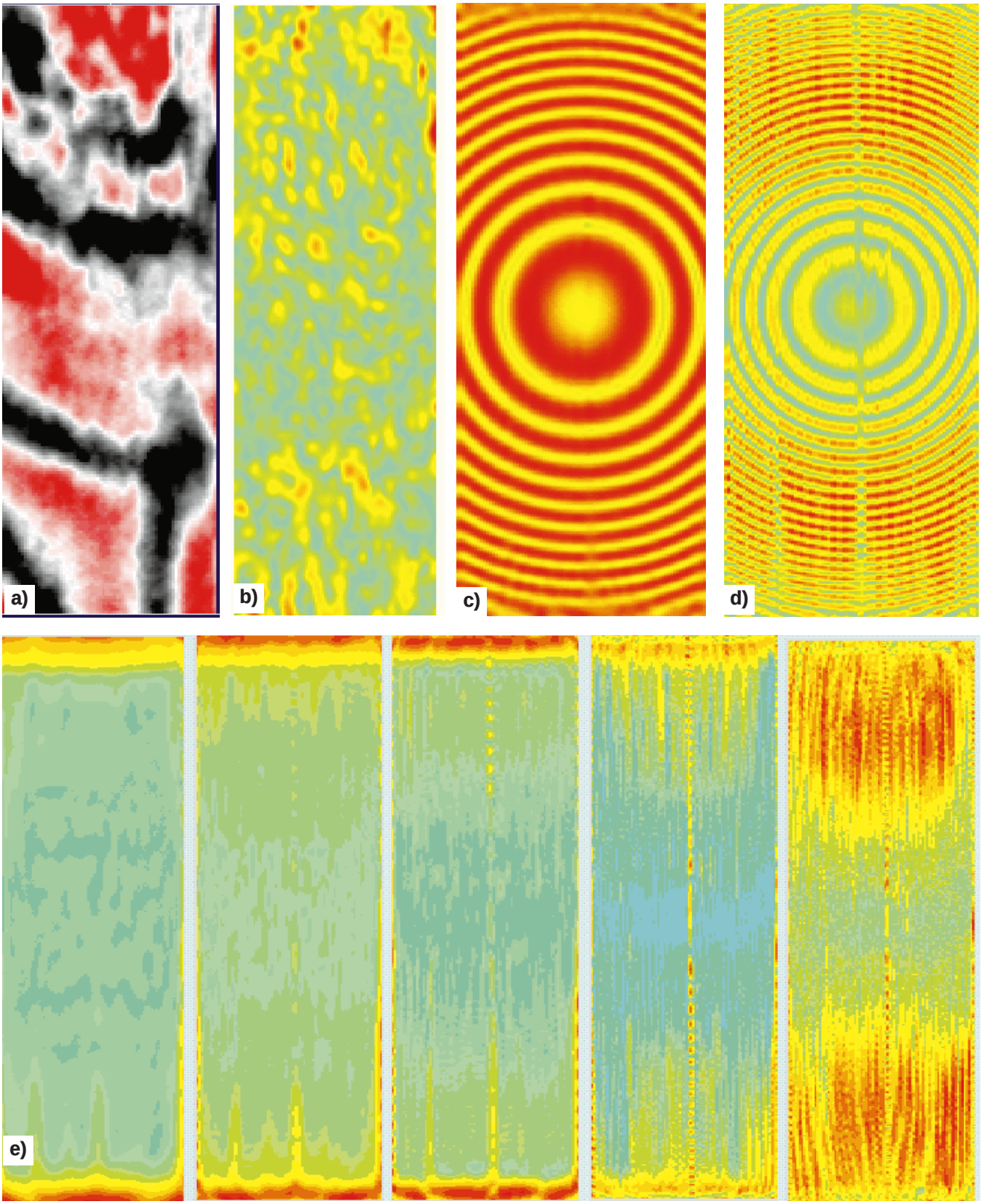

Figure 7. Bull's-eye coverage analysis: The geometry footprint depends on the processing method. From the same input data of Figure 6, IZO produces a geometry footprint-free image at low frequency and reduced geometry footprint and high frequency. This can be seen in various domains. (a) Time slice. (b) Frequency slice of real data. (c) Low-frequency slice from the IZO image of synthetic data using the real geometry. (d) High-frequency slice from the IZO image of the synthetic data using the actual real geometry. Note that at a high frequency, even IZO cannot illuminate the updip part of the gap. (e) The true solution is calculated and compared to the image at various frequencies, providing a frequency dependent QC indicator. With this choice of color table, green is acceptable, amber is marginal, and red is an illumination problem.

Downloaded 10/16/19 to 69.181.139.133. Redistribution subject to SEG license or copyright; see Terms of Use at http://library.seg.org/

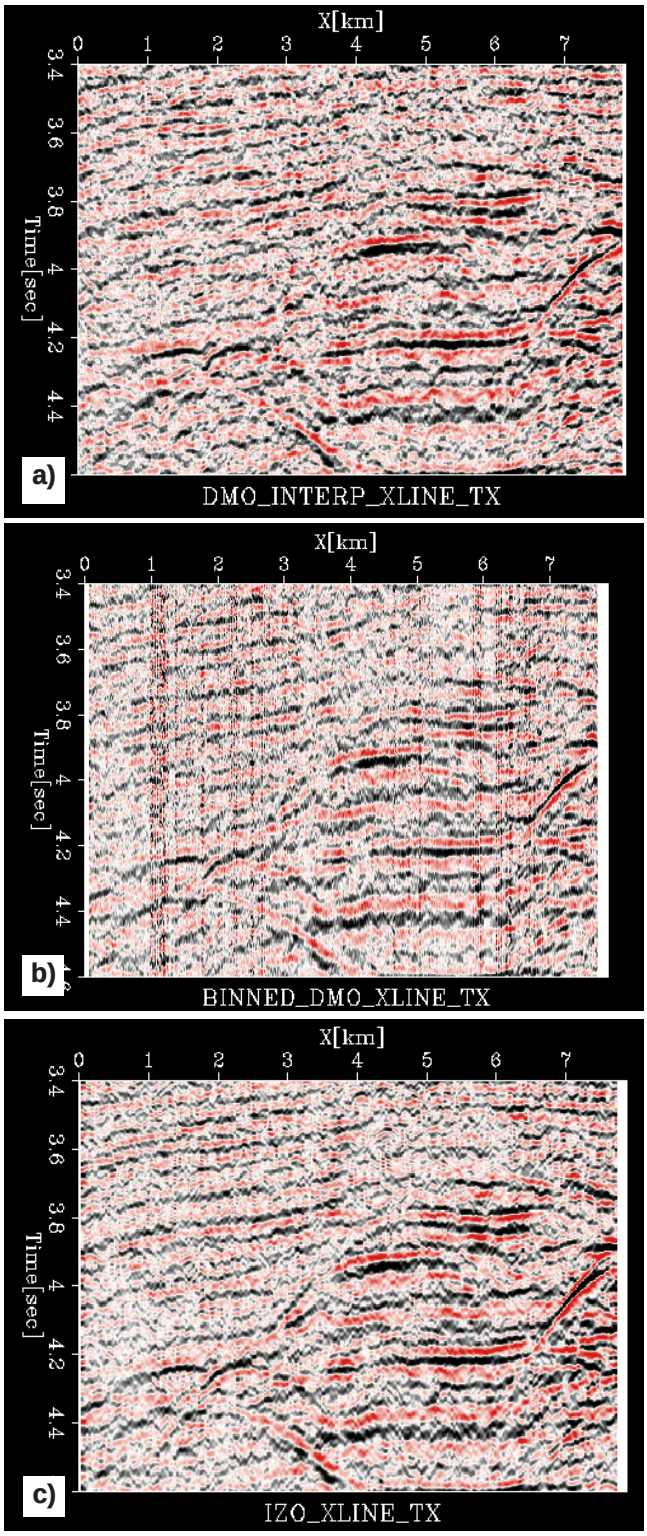

Figure 8. Comparison between images from various processing applied to the same data. (a) DMO stack binned at nominal 12.5 × 37.5 m bins and later interpolated to 12.5 m cross-line using prediction filters in the *f-xy* domain, and filtered with noise suppression with *f-xy* prediction filters. (b) DMO stack at 12.5 × 12.5 m bins and poststack *f-xy* prediction filters noise suppression. (c) IZO image generated directly at the 12.5 × 12.5 m bins. Dipping reflectors are stronger on (c) and some dipping reflectors are imaged only by IZO. In addition to the improved resolution, IZO also provides better continuity of the amplitudes of the flat reflectors.

bandwidth of the data.

Since nominal bin size and fold coverage are replaced by spatial data distribution, the traditional concept of coverage plots no longer applies. As an alternative, the data distribution can be analyzed by inverting synthetic data with the real data geometry.

The synthetic data are generated with a point diffractor and a flat reflector. With such a model, each output frequency slice should contain concentric circles that form a bull's-eye. The actual images may deviate from the ideal bull's-eye and reveal poor coverage for certain dips and azimuths as a function of frequency (Figures 6 and 7). The analysis shows the maximum temporal frequency of image on a desired output grid (i.e., one that is free of the acquisition footprint). It is believed that this QC concept better conforms to prestack processing techniques and better evaluates irregularities in the acquisition geometry.

Field navigation data for a seismic survey with a nominal bin size of 12.5 m in-line and 25 m cross-line have been input to the above bull's-eye analysis. The final data set was characterized by in-line stripes due to azimuth 3-D DMO effects, especially for sail lines in the updip direction. These can again be recognized in Figure 6, a map view image of one monochromatic low-frequency slice for a model consisting of a single point diffractor and a single flat reflector. The interference between the diffraction and the flat reflector creates the rings. The line orientation is in the x-direction. In the central part of the survey area, a broad swath of low or no coverage can be recognized. This may be caused by insufficient acquisition or by the DMO effects.

An attempt was made to obtain an image on a grid of 12.5 × 12.5 m instead of the acquisition grid of 12.5 × 25 m. The unacceptable striping in the x direction indicates that with conventional processing, the acquisition bin geometry is insufficient for this finer output grid. Figure 7 shows the IZO results and the true solution. The spatial distribution of the field data is exploited successfully to fill the smaller bins, and a width of half the subsurface line separation does not seem to be a problem.

In addition, IZO does not generate any DMO striping artifacts. However, at high frequencies, even IZO cannot produce an acceptable image. This is clear via the bull's-eyes analysis in Figure 7d.

Figure 8 compares DMO and IZO. In addition to DMO or IZO, the prestack processing sequence included deconvolution, demultiple, and for DMO *f-xy* noise suppression. In Figure 8a, bins are poststack interpolated from 37.5 to 12.5 m; in Figures 8b and 8c, images are directly generated at 12.5 m bins. The IZO section has an improved signal-to-noise ratio, and dipping data seem superior. It is tempting to interpret the dipping event on the left as the image of a fault plan. The Kx-Ky spectrum (not shown) for a time slice at target depth shows directional effects after DMO and traditional binning. The IZO with regularization does not reveal any orientation and thus confirms the omnidirectional characteristics of the regularization.

In addition to the improved structural image, the reflection amplitudes, wavelets, and derived attributes are more closely related to the rock properties. This will yield a more reliable lithological interpretation.

Suggestions for further reading. "Effects of seismic acquisition geometry on seismic processing analysis of the DMO technique" by Brink et al. (1995 EAGE Annual Meeting). "Dealiasing DMO: the good, the bad, and the unconstrained" by Ronen et al. (SEG 1995 *Expanded Abstracts*). TLE

Corresponding author: S. Ronen, shuki@slb.com

Downloaded 10/16/19 to 69.181.139.133. Redistribution subject to SEG license or copyright; see Terms of Use at http://library.seg.org/

Appendix to Coverage and binning issues for marine seismic surveys

Land data example of IZO

An oversampled land data set from Canada was decimated to simulate a more economic acquisition geometry. This article compares the results of processing the decimated data with DMO and IZO.

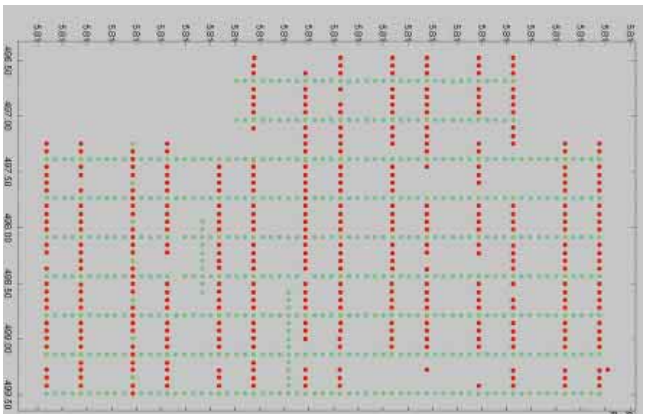

Figure 1. Map of shot and receiver points.

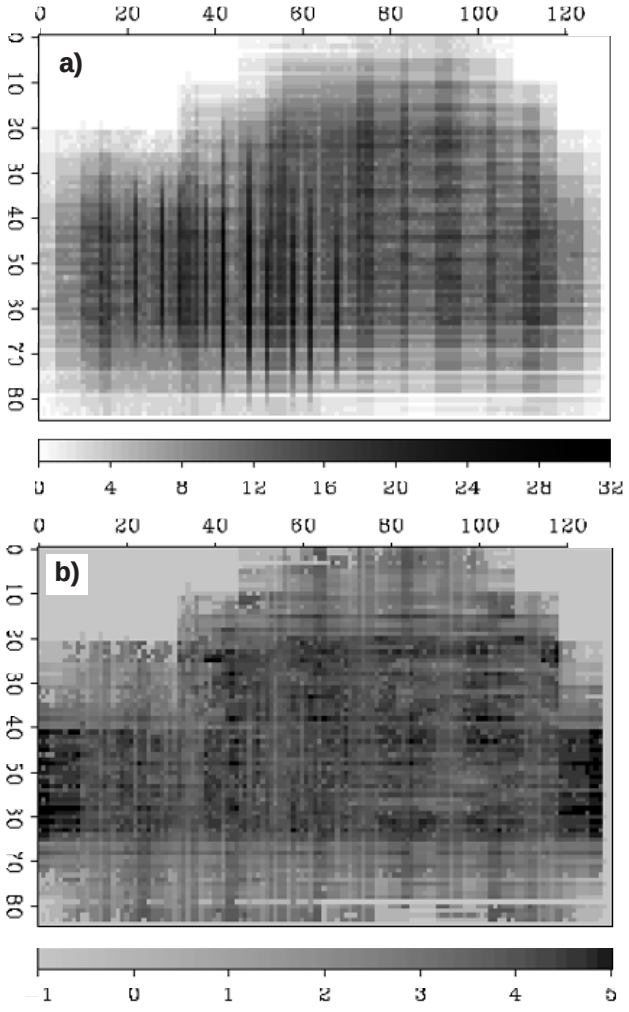

Figure 2. Maps of (a) midpoint fold and (b) offset standard deviation.

Figures 1 and 2 show the geometry of the processed data (after decimation and after removal of all traces with suspect signal-to-noise ratio). The geometry is mostly cross-spread, except two receiver lines that run parallel to the shot lines. These two lines cause some fold anomalies. The offset standard deviation is relevant to the footprint of the suppression of low-velocity multiples by stacking.

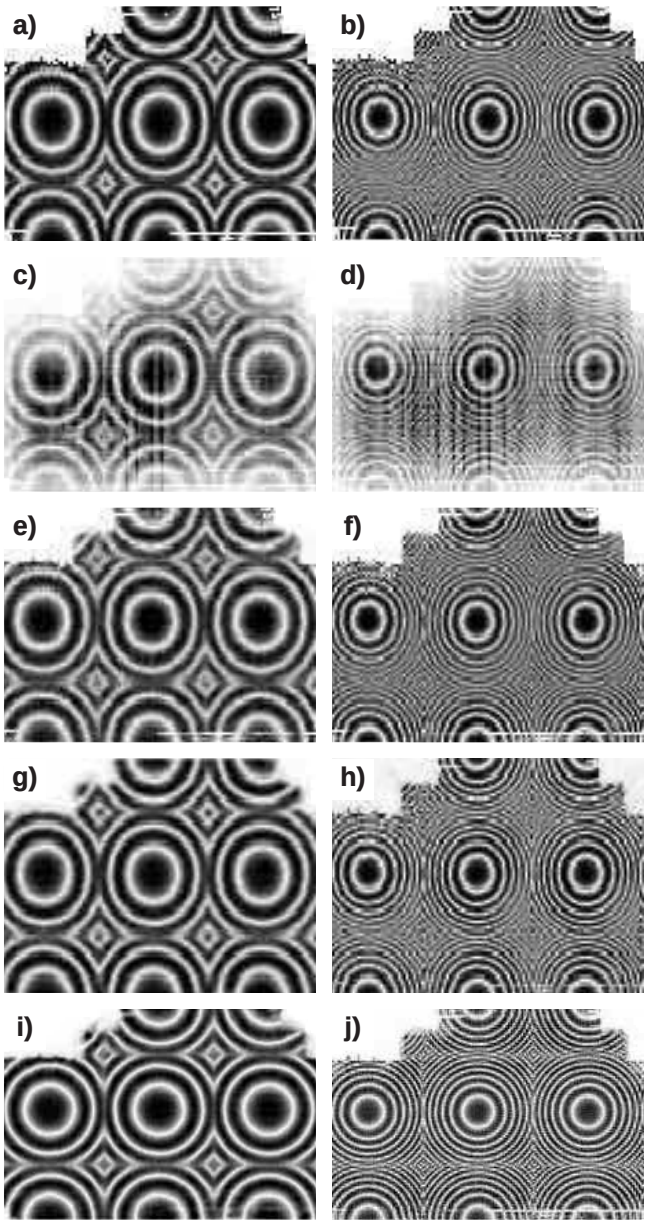

Figure 3. (a) NMO with 35-m bins, 20 Hz. (b) NMO with 35-m bins, 50 Hz. (c) DMO with 35-m bins, 20 Hz. (d) DMO with 35-m bins, 50 Hz. (e) Calibrated DMO with 35-m bins, 20 Hz. (f) Calibrated DMO with 35-m bins, 50 Hz. (g) IZO with 35-m bins, 20 Hz. (h) IZO with 35-m bins, 50 Hz. (i) IZO with 17.5-m bins, 20 Hz. (j) IZO with 17.5-m bins, 50 Hz.

Downloaded 10/16/19 to 69.181.139.133. Redistribution subject to SEG license or copyright; see Terms of Use at http://library.seg.org/

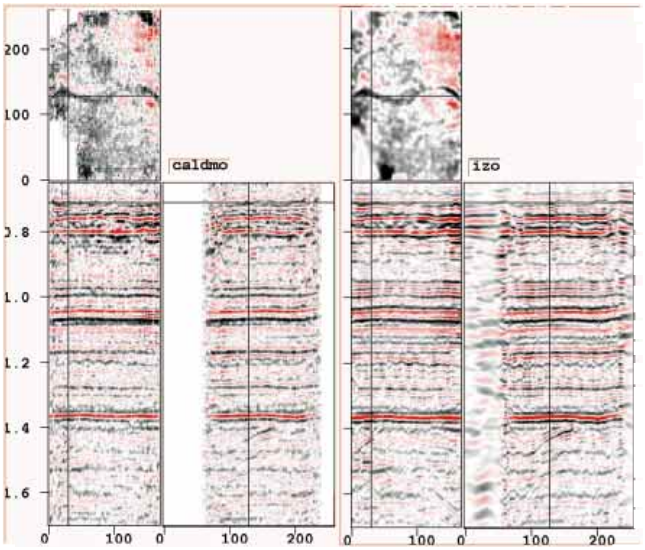

Figure 4. Calibrated DMO (left) and IZO (right). The displays are a time slice and two normal cross-sections from a data cube. The thin black lines indicate the locations of the slice and the sections.

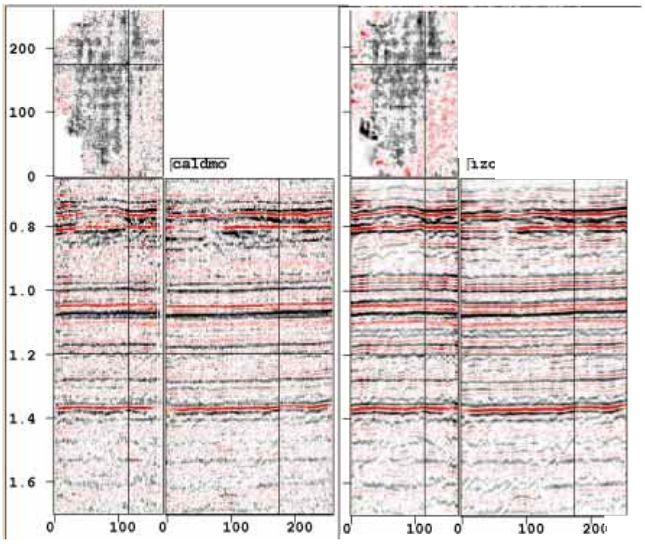

Figure 5. Other slices and sections through the same cube as Figure 4. These slices are taken on a multiple and show a footprint that is related to the map of offset standard deviation (Figure 2b). Multiples on cross-spread geometry were recently analyzed by Hampson (1998 EAGE convention); his analysis seems to agree with the identification of the footprint on the time slice at 1.2 seconds as a multiple.

Figure 3, a bull's-eye analysis, indicates that calibrated DMO is needed to equalize the coverage. With IZO, it is expected that subbinning to 17.5 m (half the nominal bin size) will provide better resolution.

The data were first processed with conventional deconvolution, velocity analysis, surface-consistent statics, and normal moveout. All traces suspected of low signal-to-noise ratio were removed. Also, all traces were balanced by the amplitude of the 98th quantile, and by clipping all values above 1 after this trace balance. (The 98th quantile is a value which is larger than 98% of the data and smaller than 2% of the data.) Following the signal-to-noise enhancing, the data

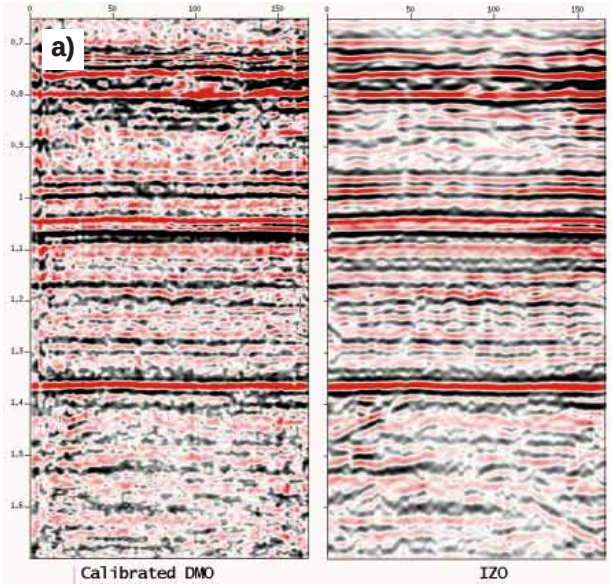

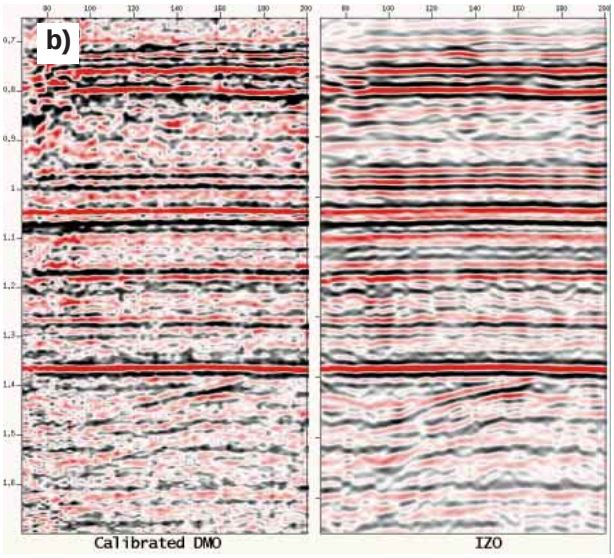

Figure 6. Cross-line sections comparing DMO to IZO at (a) y = 128 and (b) x = 30. Note the dipping reflectors at 1.4-1.6 s.

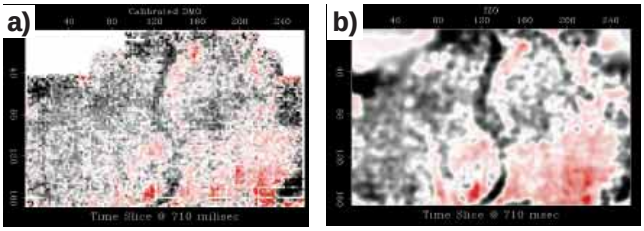

Figure 7. Time slice at 710 ms. (a) Calibrated DMO and (b) IZO. Note the effect of the half-binning (to 17.5-m) on the IZO image.

were imaged using calibrated DMO and IZO. Figures 4-7 compare these images.

—Shuki Ronen,
Geco-Prakla, Gatwick, England
—William Goodway,
Pan Canadian Petroleum, Calgary, Canada